RSC Advances

PAPER

View Article Online
View Journal | View Issue

Cite this: *RSC Adv.*, 2024, **14**, 2975

New fluorene-based bipolar charge transporting materials†

Aistė Jegorovė,*[a] Marytė Daškevičienė,[a] Kristina Kantminienė,[b] Vygintas Jankauskas,[c] Romualdas Jonas Čepas,[c] Alytis Gruodis,[c] Vytautas Getautis[a] and Kristijonas Genevičius[c]

Received 6th November 2023
Accepted 10th January 2024

DOI: 10.1039/d3ra07583d

rsc.li/rsc-advances

Air-stable and solution-processable fluorene-based bipolar charge transporting materials (CTMs) were designed, synthesized, and analyzed. These CTMs feature anthraquinone, 9-fluorenone, and 9-dicyanofluorenylidine groups and exhibit good film formation properties for solvent processing. Quantum chemistry simulations and optical absorption measurements proved that several stable conformers and charge transfer complexes form inside the molecules. Hole mobilities in CTMs were around 10^{-4} to 10^{-5} cm^2 V^{-1} s^{-1}, while electron mobility in compounds with anthraquinone and 9-dicyanofluorenylidine groups was approximately one order of magnitude lower.

Introduction

The innovative design of organic compounds and the tuning of their practical properties has become an important tool of materials science used to address major contemporary global issues, including the energy crisis and environmental impact. Therefore, the synthesis of new organic functional molecules and their adjustment for high performance materials has been gaining considerable attention in recent years. In the last few decades, the development of organic compounds as active components of electronic and optoelectronic devices, such as organic solar cells (OSCs),[1,2] dye-sensitized solar cells (DSCs),[3] organic field-effect transistors (OFET),[4–6] organic light-emitting diodes (OLEDs),[7,8] and organic photorefractive devices[9] has contributed to a significant breakthrough in their technological applications and expanded fundamental research knowledge that could be used for future scientific and technological advancement.

Electronic or optoelectronic devices that employ organic materials as active elements benefit from the important advantages of organic materials, such as their potentially low cost and light mass as well as the ability to form thin-film large-surface-area flexible devices. The first industrial-scale application of organic semiconductors was xerography.[10] Since then, charge transporting materials have played a significant role in many of the technologies that have evolved from xerography.[11] Although an extensive data on hole- or electron-transporting materials have been reported in scientific literature, molecules capable of transporting both holes and electrons have received much less attention.[12]

Different strategies have been implemented to achieve bipolar behaviour of organic materials for electronic and optoelectronic applications. Methods used to ensure bipolarity include layered heterostructure, interpenetrating network, and charge transfer complex creation.[13–16] Several disadvantages are associated with the first two of these methods, such as the increased complexity of the manufactured device; the higher probability of occurrence of defect points or nonuniformity of the layer owing to formed defective charge transfer complexes, and the possible long-term instability. In addition, it is well known that the formation of charge transfer complexes significantly reduces the charge mobility of one of the components used,[11,17] so achieving balance between the mobility of electrons and holes in the layer becomes a challenging issue. Therefore, a more reasonable approach toward bipolarity of organic materials is to design the bipolar charge transporting material (CTM) as a single compound. Thus, utilization of a bipolar material reduces both the number of mixed materials and helps maintain device stability. Additionally, it is technologically advantageous for such materials to be air-operable and soluble in common organic solvents since low-cost organic electronic or optoelectronic devices require material deposition *via* solution processes instead of expensive vacuum thermal deposition.

However, the reported number of single-component air-stable and soluble bipolar CTMs capable of transporting both carrier types is limited despite the obvious advantages of such molecules. Aso *et al.* achieved bipolar transport by attaching a hole-transporting oligothiophene unit to the fullerene core.[18]

[a]*Department of Organic Chemistry, Kaunas University of Technology, Radvilėnų pl. 19, Kaunas, 50254, Lithuania*

[b]*Department of Physical and Inorganic Chemistry, Kaunas University of Technology, Radvilėnų pl. 19, Kaunas, 50254, Lithuania*

[c]*Institute of Chemical Physics, Vilnius University, Saulėtekio al. 3, Vilnius 10257, Lithuania. E-mail: romualdas.cepas@ff.vu.lt*

† Electronic supplementary information (ESI) available. See DOI: https://doi.org/10.1039/d3ra07583d

Several other fullerene derivatives bearing, for example, dendritic oligothiophene side chains,[19] oligophenyleneethynylenes,[20] thioaxanthenes,[21] hydrazones,[22,23] or hexa-*peri*-hexabenzocoronene[24] have also been shown to exhibit bipolar behaviour, though with moderate charge-carrier mobilities. These compounds have quite complex structures and require expensive starting materials and/or elaborate multistep syntheses. Fullerene derivatives widely used as acceptors in OSCs are associated with poor absorption, high cost, and insufficient stability. As an alternative, bipolar small molecule acceptors based on the fused terthieno[3,2-*b*]thiophene or benzodithiophene donor core and various electron-withdrawing end groups have been tested in OSCs.[25,26]

Various small molecule donor materials incorporating diketopyrrolopyrrole fragment in their structure have been designed and synthesized for solution-processed optoelectronic devices.[27–33] Imide derivatives are another successful class of materials used for bipolar CTMs.[34,35] The carbazole moiety, because of its electron donating ability, is a convenient donor component of bipolar CTMs, while triazine, cyano, pyridine, phosphine oxide, *etc.* are used as acceptor fragments.[36] Velasco *et al.* investigated stable long-lived organic carbazole-based radical adducts as an electron donor–acceptor system with bipolar charge transport behaviour. High electron and hole mobilities up to 10^{-2} and 10^{-3} cm^2 V^{-1} s^{-1}, respectively, were achieved.[37,38] Kim *et al.* reported the synthesis of the bipolar hosts bearing 9,9-bis(9-alkylcarbazole)thioxanthene-*S*,*S*-dioxide moiety for application in white organic light emitting diodes. The thioxanthene-*S*,*S*-dioxide moiety possesses good electron-transporting ability, while the bis-ethylhexyl-, octyl-, dodecyl- or heptadecanylcarbazole moieties have good hole-transporting ability.[39]

Recently, we designed and synthesized air-stable and solution-processable tetracarboxydiimide-based bipolar CTMs, bearing electron-transporting 1,4,5,8-naphthalene- or 3,4,9,10-perylenetetracarboxy-diimide cores with attached 1-phenyl-1,2,3,4-tetrahydroquinoline moieties as end-capping hole-transporting groups in a straightforward and simple manner without the need for advanced synthetic procedures, expensive catalysts or sensitive reagents.[40]

Generally, soluble and air-stable bipolar CTMs have quite complex structures and require expensive starting materials and/or elaborate multistep synthesis. In this work, we have designed and synthesized air-stable and solution-processable fluorine-based bipolar materials **V1393**, **V1421**, **V1457**, **V1458**, **V1484**, and **V1485** (Fig. 1). These CTMs were obtained from inexpensive starting materials through simple reactions and possess electron transporting anthraquinone, 9-fluorenone, or 9-dicyanofluorenylidine with attached carbazolyl electron-donating moieties. The optical, thermal, and charge carrier transport properties of the synthesized CTMs were studied. The existence of possible conformers and excitation energies were calculated by the means of quantum chemistry simulations.

Results and discussion

Target bipolar molecules were synthesized *via* the synthetic route depicted in Scheme 1. The precursors (side-amines) were synthetized by coupling 3-bromo-9-ethylcarbazole with 2-aminoantraquinone and 2-amino-9*H*-fluorenone. The target compounds **V1393**, **V1421**, **V1457**, and **V1458** were synthesized under Buchwald–Hartwig amination reaction conditions using a central fluorene-based core as the starting material. The dicyanofluorenylidine derivatives **V1484** and **V1485** were synthesized by modifying the keto group to malononitrile by Knoevenagel condensation in basic medium.

The chemical structures of the synthesized compounds were verified by NMR spectroscopy, mass spectrometry, elemental analysis, and infrared spectroscopy data. A detailed description of the synthetic procedures and analysis is presented in the ESI.†

Thermal stability of new bipolar molecules was evaluated by thermogravimetric analysis (TGA) in nitrogen atmosphere (Fig. 2). As seen from the data presented in Table 1 and Fig. 2, all

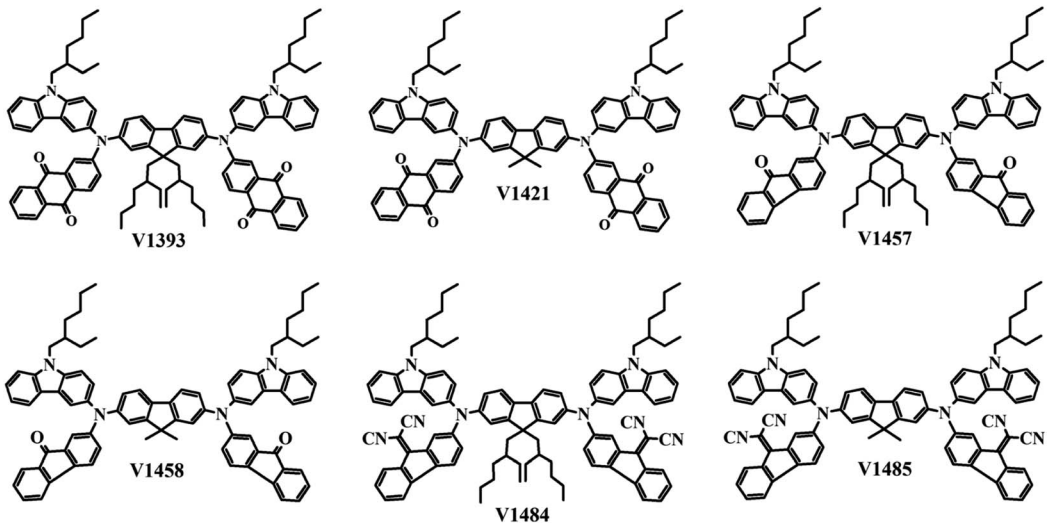

Fig. 1 Chemical structures of the synthesized bipolar compounds bearing different structural units.

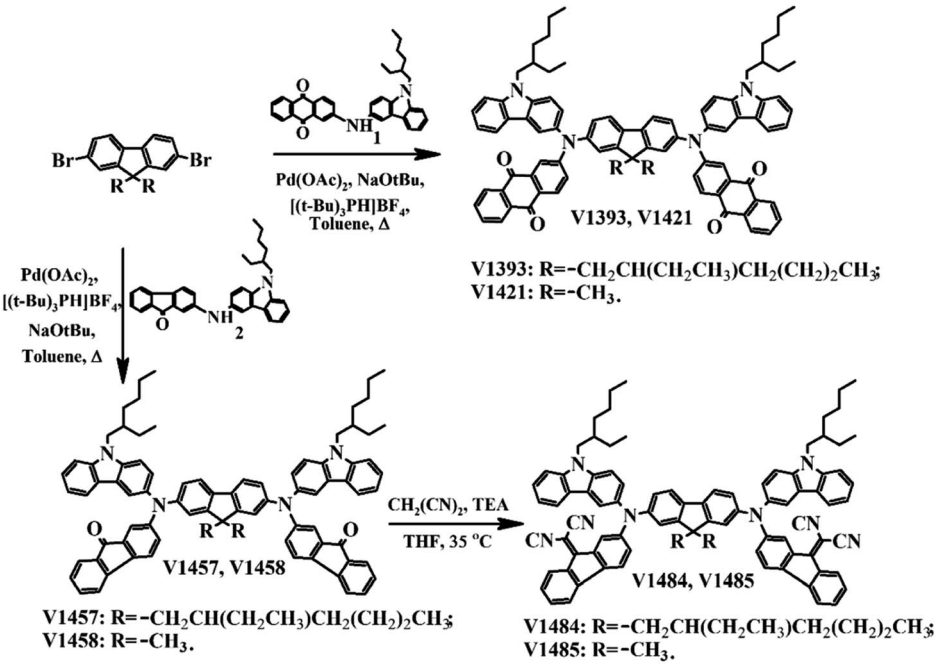

Scheme 1 Synthesis of new fluorene-based bipolar compounds **V1393**, **V1421**, **V1457**, **V1458**, **V1484**, and **V1485**.

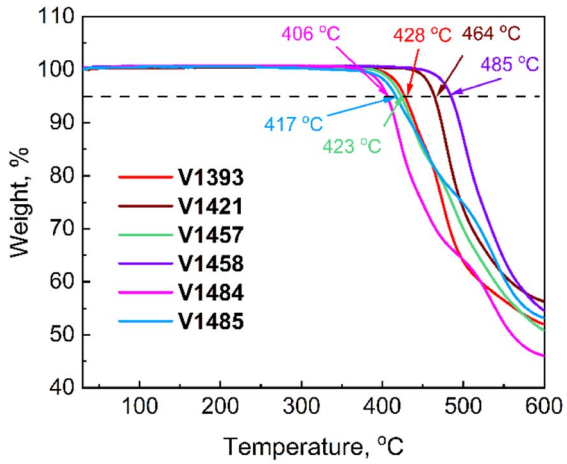

Fig. 2 TGA curves of new bipolar molecules.

bipolar compounds are thermally stable at temperatures higher than 400 °C that is well above operating temperatures of most electronic devices.

The results of differential scanning calorimetry (DSC) measurements are shown in Fig. 3. According to the DSC scans, the glass transition temperatures (T_g) were observed at 109 and 153 °C for **V1393** and **V1421**, respectively. Notably, the T_g of **V1457** and **V1458** are lower than those of their analogues with anthraquinone moieties (92 °C for **V1457** and 133 °C for **V1458**). The glass transition temperatures increased when the cyano groups were incorporated into the molecules (112 °C for **V1484** and 161 °C for **V1485**). Furthermore, as expected, all materials with longer alkyl side chains demonstrated lower glass transition temperatures than those of the ones with shorter alkyl chains. No endothermic peaks were observed during two heating cycles, what proves that all new materials are amorphous. It is preferable that new bipolar molecules would have an amorphous state in order to obtain good quality films.

For obtaining more information about electronic structure, quantum chemistry simulations of the molecular structure and several most probable conformers as well as dimers were performed using Gaussian 16 software.[41] The density functional (DFT) Cam-B3LYP method and the 6-31G (d) basis set supplemented with polarization functions (d,p) were used for ground state optimization. Solvation effects were not considered in all cases. The list of two most probable molecular conformations is presented in the ESI, Table S1† and *xy* projections are in Fig. S2–S4.† Generally, total molecular symmetry is absent in the analyzed structures, but in several cases partial symmetry (or quasi-symmetry according to central fluorene unit) could be established (for example, **V1421b**, **V1458b**, and **V1485b**). Substituents are oriented in a chaotic manner, and large number of different conformers could be obtained. The population of low-lying excited molecular states S_1 and S_2 could be realized using the partially allowed transitions $S_0 \rightarrow S_n$, $n = 1, 2$ (Table S2†). The parameters of transition between MO (which are related to the population of "spectroscopic" states S_n, $n = 1$, 2) are presented in the ESI, Table S3.† In all cases, the dominant and most significant electron jump is provided between HOMO and LUMO. Spatial distributions of electron density (for the HOMO-1, HOMO, LUMO and LUMO+1 of each compound) are presented in the ESI, Tables S4–S6.† Generally, electron transition between HOMO and LUMO corresponds to the charge redistribution between the core (fluorene) and substituents (for example, anthraquinone). In case of both conformers of **V1421** and **V1393**, by population of the lowest excited state, charge

Table 1 Thermal, optical, and photophysical properties of the bipolar compounds

Compound	T_g[a] [°C]	T_{d5}[a] [°C]	λ_{abs}[b] [nm]	I_p[c] [eV]	HOMO[d] [eV]	LUMO[e] [eV]	$\mu_{0\ hole}$[f] [$cm^2\ V^{-1}\ s^{-1}$]	$\mu_{0\ elec.}$[g] [$cm^2\ V^{-1}\ s^{-1}$]
V1393	109	428	311, 355, 512	5.18	5.38	3.85	2.6×10^{-7}	4.6×10^{-9}
V1421	153	464	311, 352, 514	5.21	5.51	4.0	1.4×10^{-7}	1.1×10^{-9}
V1457	92	423	378, 534	5.02	5.34	3.97	3.9×10^{-7}	—
V1458	133	485	377, 537	5.02	5.46	4.09	9.2×10^{-8}	—
V1484	112	406	337, 346, 760	5.18	5.54	4.16	1.2×10^{-7}	1.0×10^{-8}
V1485	161	417	337, 750	5.16	5.42	4.09	2.8×10^{-8}	3.5×10^{-9}

[a] Glass transition (T_g) and 5% weight loss (T_{d5}) temperatures recorded from DSC and TGA, respectively (10 °C min^{-1}, N_2 atmosphere). [b] UV-vis spectra were measured from thin layers. [c] Ionization energies of the films were measured using PESA. [d] HOMO energy levels were estimated from the CV measurements. [e] LUMO energy levels were estimated from the CV measurements. [f] Hole mobility value at zero field strength. [g] Electron mobility value at zero field strength.

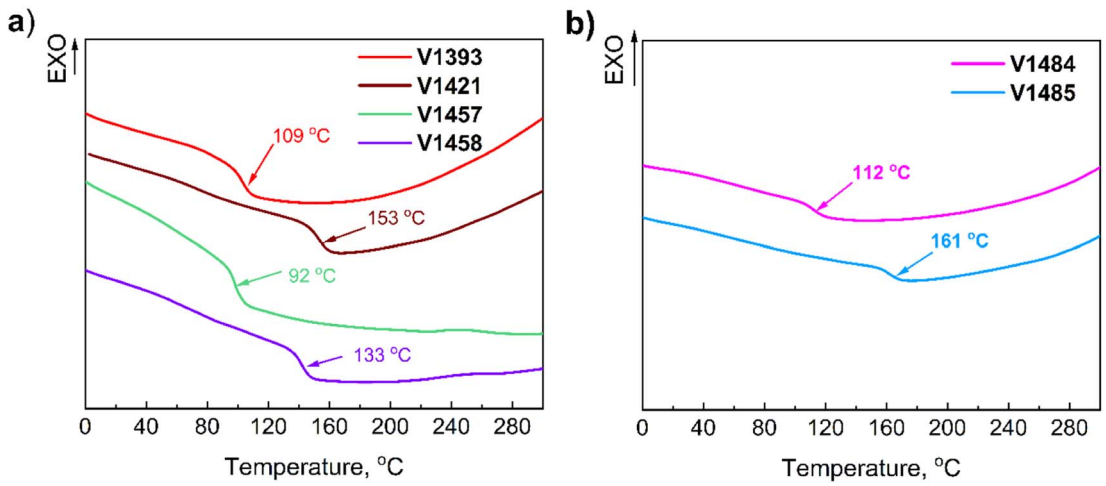

Fig. 3 DSC curves for the second run of the bipolar molecules bearing (a) carbonyl groups (**V1393**, **V1421**, **V1457** and **V1458**) and (b) cyanoylidene moieties (**V1484** and **V1485**) (heating rate of 10 °C min, N_2 atmosphere).

redistribution could be named as the closest to that of pure CT. Substituents are present in the role of electron acceptor (charge donor) (Table S4†). The tendencies for both conformers of **V1458** and **V1457** are the same. The HOMO orbital is localized in the central fluorene unit and in well-oriented substituents (Table S5†). Small changes occur for both conformers of **V1485** and **V1484**. The chaotic orientation of the 2-ethylhexyl- fragment related to the central fluorene unit predetermines the strong non-symmetric displacement of the substituents (Table S6†). Due to that, only the left part of **V1484a** is involved in significant charge redistribution by excitation.

To understand the nature of electronic excitations, we decided to provide the natural transition orbitals (NTO) analysis using Gaussian16 routine: Density=(Check, Transition=1,2) Pop=(NTO, SaveNTO) for first and second transitions. HOMO and LUMO NTO (which correspond the electronic densities of hole and electron NTO pairs) for allowed first transition are presented in ESI, Tables S7–S9.†

List of several most probable molecular dimers is presented in ESI, Table S10.† Two typical structures in most informative projections are presented in Fig. S23.† First structure of open V-shaped type (dimmer **Eh0**, V1421b + V1421b) presents amorphous behaviour of low density condensed phase. Intermolecular structure could be organized using weak van-der Waals forces, which relates two molecules through substituents. Second structure of core-to-core type (dimmer **Eh2**, V1458b + V1458b) represents amorphous behaviour of high density condensed phase. Intermolecular structure could be organized overlap of central core unit of different molecules. Additional relations of two molecules are organized through the substituents. Orientation of two core units is not parallel, but closed to perpendicular (dehidral angle −20 deg).

A comparison of the UV-visible absorption spectra of the new HTMs recorded in THF solution and from solid films is shown in Fig. 4, and the corresponding data are listed in Table 1.

In general, the spectra of all target compounds display not less than three absorption bands. As expected, the same group molecules, which structures differ in the length of the alkyl chains, present similar absorption profiles from 250 to 900 nm. The spectra of all new compounds display an intensive π–π* absorption bands at 270–450 nm, while the weak absorption band with maximum in the visible region has *n*–π* nature. While comparing spectra of **V1393**, **V1421**, and **V1457**, **V1458** the red shifted absorption peaks can be detected. Stronger absorption for **V1393**, **V1421** around 510 nm is attributed to the presence of additional oxygen atoms. The same phenomenon

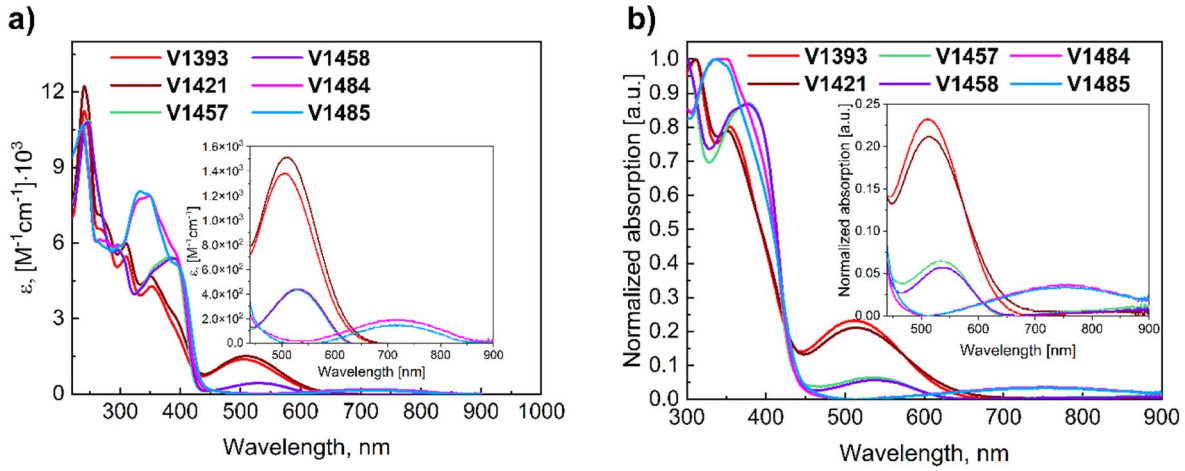

Fig. 4 UV-vis spectra of the target compounds from (a) THF solutions ($c = 10^{-4}$ mol l^{-1}); (b) solid films.

was observed when dicyanoylide groups were added to the molecule.

When compared to the solution samples, the absorption of film samples exhibits a minimal red shift (~3 nm) (Fig. 4b), suggesting a significant degree of intermolecular interactions in the solid state. Additionally, this shift supports the presence of aggregates even in low-concentration solutions. Quantum chemistry calculations further validated these findings, indicating that such intermolecular transitions were only feasible in dimer structures. The photoluminescence (PL) measurements were conducted on the solutions and solid layers of materials, but no observable emission was detected.

To assess the energy levels of novel bipolar molecules, their oxidation (E_{ox}) and reduction (E_{red}) potentials in solution and ionization potential (I_p) values in the solid-state were determined using cyclic voltammetry (CV) and photoelectron spectroscopy in air (PESA) techniques, respectively. The experimental results are depicted in Fig. 5, S19,† and Table 1. Materials with anthraquinone moieties have the highest I_p values (5.18 and 5.21 eV for **V1393** and **V1421**, respectively). As expected, the alkyl chain attached to the 9-fluorenyl core practically does not affect I_p. The comparison between molecules containing anthraquinone fragment and molecules containing fluoren-9-one chromophores has revealed compelling evidence that a decrease in the number of electron-withdrawing keto groups within the molecule leads to a reduction in the ionization potential. The opposite effect, *i.e.* increase of the I_p values, was recorded when cyanoylidene fragments were present in the molecule instead of the keto groups. The inclusion of additional electron-acceptor fragments or strengthening them in this concept resulted in an increase in the ionization potential values.

The CV measurements (Fig. S19†) have clearly indicated that materials containing anthraquinone exhibit two oxidation peaks and two reduction peaks in a positive region, while compounds incorporating the fluoren-9-one and cyanoylidene groups display three peaks corresponding to oxidation and reduction processes. Comparison of **V1393**, **V1421** with **V1457**,

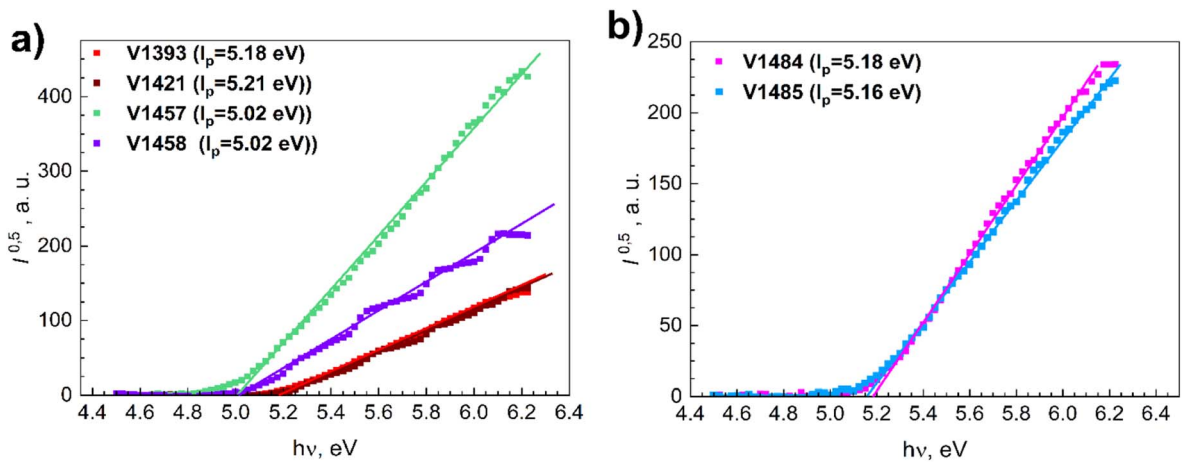

Fig. 5 Photoemission in air spectra of new compounds with (a) carbonyl groups (**V1393**, **V1421**, **V1457**, and **V1458**) and (b) cyanoylidene substituents (**V1484** and **V1485**).

V1458 has apparently revealed that reducing the number of oxygen atoms in the molecule results in a slight decrease in the oxidation potential (E_{ox}) value. Other modifications in the structures have a minimal effect on the E_{ox} values.

The CV of the analyzed compounds has demonstrated reversible reduction during the scanning process in a negative region, indicating the electrochemical stability of the synthesized materials. It is important to note that these values do not represent absolute electron affinity or ionization energies in the solid state, but they can be utilized to compare different compounds relative to each other. The estimated ranges for the LUMO and HOMO energy levels of the novel compounds were found to be between −3.85 eV and −4.16 eV, and between −5.02 eV and −5.21 eV, respectively.

The hole and electron mobility is a fundamental parameter when bipolar molecules are evaluated. To analyze the charge transport properties of novel compounds, time-of-flight measurements (XTOF) were employed; the transient signals are presented in the ESI, Fig. S24–S29.† These measurements were conducted in films of the pure compounds, and the obtained mobility dependencies on electrical field are presented in Fig. 6.

The results have clearly indicated that molecules containing anthraquinone fragments (**V1393**, **V1421**) and cyanoylidene substituents (**V1484**, **V1485**) exhibit both negative and positive charge transport capabilities with hole mobility reaching values of one order of magnitude higher than those of electrons. However, no electron-clear transients were obtained in compounds **V1457** and **V1458** bearing 9-fluorenone chromophores as electron acceptors. The only noticeable effect of longer alkyl chains (**V1393**, **V1457**, and **V1484**) was a slight improvement of hole mobilities at low electric fields, thus a case could be made that longer alkyl chains may be beneficial for more optimal molecular arrangement for charge transport. Replacement of the keto groups with cyanoylidene groups resulted in decreased hole drift mobility and increased electron mobility. The most balanced charge mobility has been recorded in the bipolar molecules **V1484** and **V1485**, where the hole mobility is 1.2×10^{-7} cm^2 V^{-1} s^{-1}, and the electron mobility is 1.0×10^{-8} V^{-1} s^{-1} at near zero electric fields.

Photocurrent decay measurements were conducted to gain deeper insights into charge transport within the layers. The applied electrical field was insufficient to facilitate the extraction of charge carriers from the layer, causing photocurrent decay to be predominantly influenced by

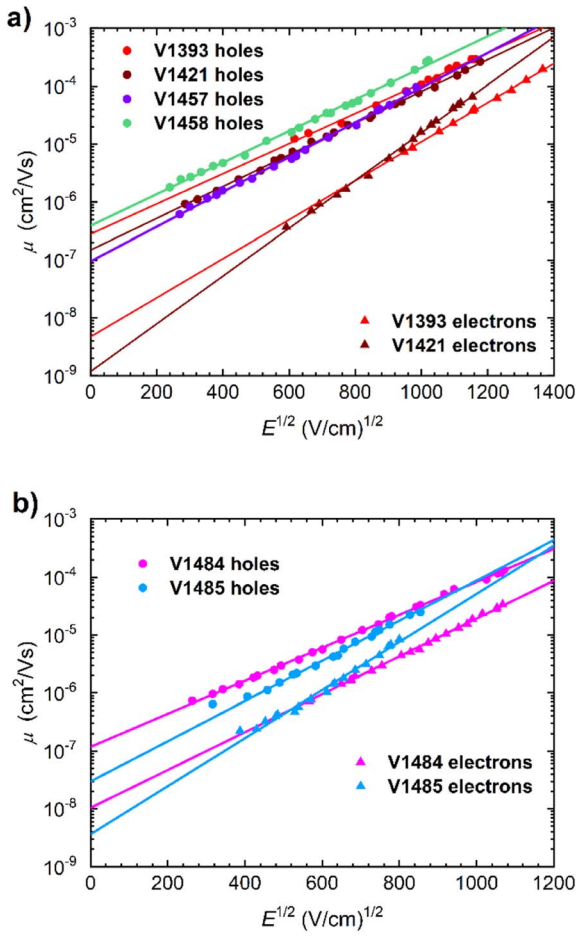

Fig. 6 Electric field dependencies of the new materials containing (a) anthraquinone and fluorenone functional groups (**V1393**, **V1421**, **V1457**, and **V1458**) and (b) cyanoylidene group (**V1484** and **V1485**).

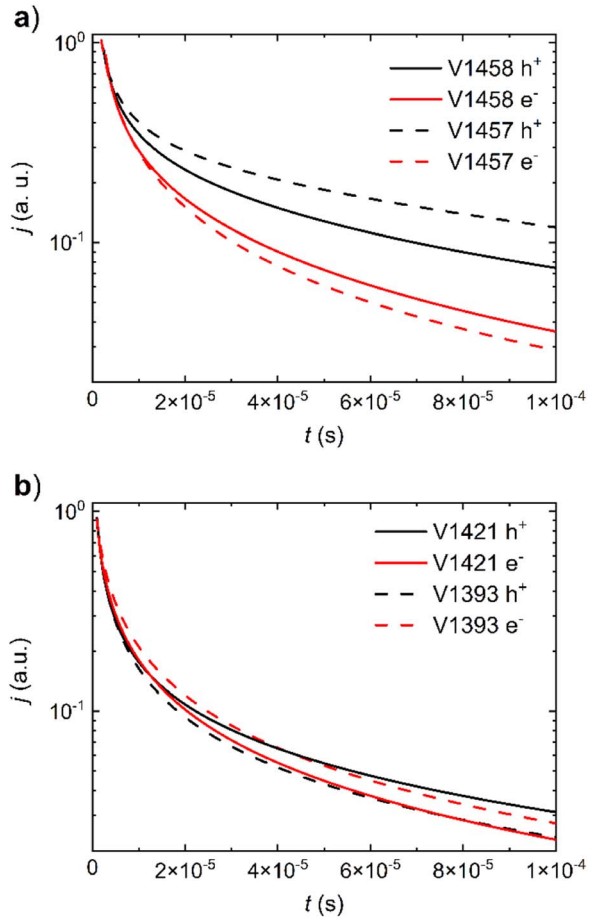

Fig. 7 Photocurrent decay profiles of compound films containing (a) fluorenone functional groups (**V1457** and **V1458**) and (b) anthraquinone groups (**V1393** and **V1421**).

charge carrier trapping, detrapping, and recombination processes.[42,43]

The resulting profiles were normalized to compare the photocurrent tail regions of decay (ranging from 2×10^{-5} to 1×10^{-4} s), which primarily were attributed to deep traps and recombination mechanisms. In layers featuring anthraquinone fragments (Fig. 7b), the photocurrent decay profiles for both holes and electrons exhibit similar kinetics with minimal observable impact from additional alkyl groups. On the contrary, the most significant alterations in the slower decay region were observed when altering the length of the alkyl chains in compounds containing fluorenone groups (**V1458**, **V1457**) (Fig. 7a). The lengthening of the alkyl chains resulted in a reduced influence of trapping and detrapping on hole transport and increased recombination, as evidenced by the significantly lower hole mobilities observed in **V1458**. However, electron photocurrent decay seemed to exhibit only marginal sensitivity to the same alkyl chain modifications. Compounds featuring cyanoylidine fragments (**V1484**, **V1485**) (Fig. S30†) displayed a similar improvement when additional alkyl chains were introduced. This led to slower electron photocurrent decay alongside higher electron mobilities. These findings underscore the importance of additional alkyl groups in optimizing the molecular arrangement within the layer, subsequently enhancing charge carrier transport. Notably, the discernible differences in hole and electron current decays corroborate the discrepancies found in charge carrier mobilities.

Conclusions

New amorphous bipolar fluorine-based materials featuring anthraquinone, 9-fluorenone, or 9-dicyanofluorenylidine groups along with attached carbazolyl electron-donating moieties have been developed and synthesized *via* a straightforward synthesis. These amorphous materials exhibit homogeneous, cohesive, and continuous film-formation properties for solvent processing. Optical absorption and quantum chemistry simulations have confirmed the formation of a CT complex within the molecule, along with the emergence of a few of the most probable dimer structures, specifically V-type and core-to-core type structures. According to quantum chemistry calculations, several stable conformers are possible due to a complex geometry of the molecules.

The hole mobility in all materials is around 10^{-4}-10^{-5} cm^2 V^{-1} s^{-1}, while the electron mobility in compounds with anthraquinone and 9-dicyanofluorenylidine groups is approximately one order of magnitude lower. Electron transport in compounds with 9-fluorenone was highly dispersive and clear kink in photocurrent was not observed.

Author contributions

Aistė Jegorovė: writing – original draft, synthesis and characterization of materials; Marytė Daškevičienė: conceptualization, synthesis and characterization of materials; Kristina Katminienė: writing – original draft; Vygintas Jankauskas: project administration, supervision, investigation; Romualdas Jonas Čepas: investigation, formal analysis, visualization, writing – original draft; Alytis Gruodis: formal analysis, investigation; Vytautas Getautis: conceptualization, supervision; Kristijonas Genevičius: investigation, formal analysis, writing – review & editing.

Conflicts of interest

The authors declare no conflict of interest.

Acknowledgements

This research was funded by a grant (No. S-MIP-22-8) from the Research Council of Lithuania. Computations were performed on resources at the High Performance Computing Center "HPC Saulėtekis" (Faculty of Physics, Vilnius University, Lithuania). Dr E. Kamarauskas is acknowledged for ionisation potential measurements.

References

1 A. Bessette and G. S. Hanan, *Chem. Soc. Rev.*, 2014, **43**, 3342–3405.
2 A. Wadsworth, M. Moser, A. Marks, M. S. Little, N. Gasparini, C. J. Brabec, D. Baran and I. McCulloch, *Chem. Soc. Rev.*, 2019, **48**, 1596–1625.
3 A. B. Muñoz-García, I. Benesperi, G. Boschloo, J. J. Concepcion, J. H. Delcamp, E. A. Gibson, G. J. Meyer, M. Pavone, H. Pettersson, A. Hagfeldt and M. Freitag, *Chem. Soc. Rev.*, 2021, **50**, 12450–12550.
4 M. Chen, L. Yan, Y. Zhao, I. Murtaza, H. Meng and W. Huang, *J. Mater. Chem. C*, 2018, **6**, 7416–7444.
5 H. Jiang, S. Zhu, Z. Cui, Z. Li, Y. Liang, J. Zhu, P. Hu, H.-L. Zhang and W. Hu, *Chem. Soc. Rev.*, 2022, **51**, 3071–3122.
6 Y. Weng, Z. Yu, T. Wu, L. Liang and S. Liu, *New J. Chem.*, 2023, **47**, 5086–5109.
7 A. J. Shahnawaz, S. S. Swayamprabha, M. R. Nagar, R. A. K. Yadav, S. Gull, D. K. Dubey and J.-H. Jou, *J. Mater. Chem. C*, 2019, **7**, 7144–7158.
8 M. Sheokand, Y. Rout and R. Misra, *J. Mater. Chem. C*, 2022, **10**, 6992–7017.
9 K.-L. Wang, J.-C. Jiang, C.-H. Jhu, S. Wada, T. Sassa and M. Horie, *J. Mater. Chem. C*, 2020, **8**, 13357–13367.
10 D. S. Weiss, *J. Imaging Sci. Technol.*, 2016, **60**, 1–24.
11 D. S. Weiss and M. Abkowitz, *Chem. Rev.*, 2010, **110**, 479–526.
12 Y. Zhang, Y. Wang, C. Gao, Z. Ni, X. Zhang, W. Hu and H. Dong, *Chem. Soc. Rev.*, 2023, **52**, 1331–1381.
13 E. J. Meijer, D. M. de Leeuw, S. Setayesh, E. van Veenendaal, B.-H. Huisman, P. W. M. Blom, J. C. Hummelen, U. Scherf and T. M. Klapwijk, *Nat. Mater.*, 2003, **2**, 678–682.
14 C. Rost, D. J. Gundlach, S. Karg and W. Rieß, *J. Appl. Phys.*, 2004, **95**, 5782–5787.
15 T. D. Anthopoulos, D. M. de Leeuw, E. Cantatore, S. Setayesh, E. J. Meijer, C. Tanase, J. C. Hummelen and P. W. M. Blom, *Appl. Phys. Lett.*, 2004, **85**, 4205–4207.
16 A. Dodabalapur, H. E. Katz, L. Torsi and R. C. Haddon, *Science*, 1995, **269**, 1560–1562.

17 Y. Yamaguchi, T. Fujiyama, H. Tanaka and M. Yokoyama, *Denshi Shashin Gakkaishi*, 1991, **30**, 274–281.
18 Y. Kunugi, K. Takimiya, N. Negishi, T. Otsubo and Y. Aso, *J. Mater. Chem.*, 2004, **14**, 2840–2841.
19 N. Negishi, Y. Ie, H. Tada, T. Kaneda and Y. Aso, *Chem. Lett.*, 2007, **36**, 544–545.
20 J.-F. Nierengarten, T. Gu, T. Aernouts, W. Geens, J. Poortmans, G. Hadziioannou and D. Tsamouras, *Appl. Phys. A*, 2004, **79**, 47–49.
21 S. Amriou, A. Mehta and M. R. Bryce, *J. Mater. Chem.*, 2005, **15**, 1232–1234.
22 S. Urnikaite, T. Malinauskas, V. Gaidelis, V. Jankauskas and V. Getautis, *Chem.–Asian J.*, 2012, **7**, 614–620.
23 S. Urnikaite, T. Malinauskas, V. Gaidelis, R. Maldzius, V. Jankauskas and V. Getautis, *Carbon*, 2011, **49**, 320–325.
24 W. W. H. Wong, D. Vak, Th. B. Singh, S. Ren, C. Yan, D. J. Jones, I. I. Liaw, R. N. Lamb and A. B. Holmes, *Org. Lett.*, 2010, **12**, 5000–5003.
25 Y. Chen, T. Liu, H. Hu, T. Ma, J. Y. L. Lai, J. Zhang, H. Ade and H. Yan, *Adv. Energy Mater.*, 2018, **8**, 1801203.
26 L. Gao, Z.-G. Zhang, H. Bin, L. Xue, Y. Yang, C. Wang, F. Liu, T. P. Russell and Y. Li, *Adv. Mater.*, 2016, **28**, 8288–8295.
27 Y. Zhang, C. Kim, J. Lin and T.-Q. Nguyen, *Adv. Funct. Mater.*, 2012, **22**, 97–105.
28 L. Wang, X. Zhang, H. Tian, Y. Lu, Y. Geng and F. Wang, *Chem. Commun.*, 2013, **49**, 11272–11274.
29 A. Riaño, P. M. Burrezo, M. J. Mancheño, A. Timalsina, J. Smith, A. Facchetti, T. J. Marks, J. T. L. Navarrete, J. L. Segura, J. Casado and R. P. Ortiz, *J. Mater. Chem. C*, 2014, **2**, 6376–6386.
30 T. Bura, N. Leclerc, R. Bechara, P. Lévêque, T. Heiser and R. Ziessel, *Adv. Energy Mater.*, 2013, **3**, 1118–1124.
31 Y. Lin, L. Ma, Y. Li, Y. Liu, D. Zhu and X. Zhan, *Adv. Energy Mater.*, 2013, **3**, 1166–1170.
32 H. Bai, P. Cheng, Y. Wang, L. Ma, Y. Li, D. Zhu and X. Zhan, *J. Mater. Chem. A*, 2013, **2**, 778–784.
33 H. Shi, W. Fu, M. Shi, J. Ling and H. Chen, *J. Mater. Chem. A*, 2015, **3**, 1902–1905.
34 Q. Wu, L. Li, J. Hai, X. Zhang, Z. Lu, J. Yang, Y. Liu, L. Zhang and C. Zhan, *Dyes Pigm.*, 2016, **132**, 41–47.
35 G. Balaji, T. S. Kale, A. Keerthi, A. M. Della Pelle, S. Thayumanavan and S. Valiyaveettil, *Org. Lett.*, 2011, **13**, 18–21.
36 Y. Wang, J. H. Yun, L. Wang and J. Y. Lee, *Adv. Funct. Mater.*, 2021, **31**, 2008332.
37 M. Reig, C. Gozálvez, V. Jankauskas, V. Gaidelis, J. V. Grazulevicius, L. Fajarí, L. Juliá and D. Velasco, *Chem.–Eur. J.*, 2016, **22**, 18551–18558.
38 A. Bobet, A. Cuadrado, L. Fajarí, I. Sirés, E. Brillas, M. P. Almajano, V. Jankauskas, D. Velasco and L. Juliá, *J. Phys. Org. Chem.*, 2019, **32**, e3974.
39 K. S. Kim, D. U. Kim, K. S. Joung and J.-W. Yu, *Thin Solid Films*, 2020, **696**, 137781.
40 M. Daskeviciene, S. Urnikaite, G. Planciunaite, T. Malinauskas, A. Gruodis, M. Viliunas, E. Kamarauskas, V. Gaidelis, V. Jankauskas and V. Getautis, *Dyes Pigm.*, 2018, **158**, 157–164.
41 *Citation | Gaussian.com*, **https://gaussian.com/citation/**, (accessed October 26, 2023).
42 S. Valouch, M. Nintz, S. W. Kettlitz, N. S. Christ and U. Lemmer, *IEEE Photonics Technol. Lett.*, 2012, **24**, 596–598.
43 C. R. McNeill, I. Hwang and N. C. Greenham, *J. Appl. Phys.*, 2009, **106**, 024507.